

Atmospheric Refraction Path Integrals in Ground-Based Interferometry

Richard J. Mathar

Sterrewacht Leiden, Leiden University, Postbus 9513, 2300 RA Leiden, The Netherlands

mathar@strw.leidenuniv.nl

ABSTRACT

The basic effect of the earth's atmospheric refraction on telescope operation is the reduction of the true zenith angle to the apparent zenith angle, associated with prismatic aberrations due to the dispersion in air. If one attempts coherent superposition of star images in ground-based interferometry, one is in addition interested in the optical path length associated with the refracted rays. In a model of a flat earth, the optical path difference between these is not concerned as the translational symmetry of the setup means no net effect remains.

Here, I evaluate these interferometric integrals in the more realistic arrangement of two telescopes located on the surface of a common earth sphere and point to a star through an atmosphere which also possesses spherical symmetry. Some focus is put on working out series expansions in terms of the small ratio of the baseline over the earth radius, which allows to bypass some numerics which otherwise is challenged by strong cancellation effects in building the optical path difference.

Subject headings: Atmospheric Refraction; Optical Interferometry; Baseline; Spherical Geometry; Zenith

1. Pointing and Apparent Star Altitudes

1.1. Basics: Flat Earth Model

The standard model of an interferometric setup and delay line correction for a star at the true zenith angle z is shown in Fig. 1: The optical path difference (OPD) D shows up once in the vacuum above telescope 1, and is added for telescope 2 on the ground at some local index of refraction. The atmosphere is horizontally homogeneous and the earth flat; therefore no correction is needed for the ray path curvature induced by any vertical gradient of the index of refraction through the atmosphere, because these two paths match each other at each height above ground.

The pointing difference R between the apparent and actual altitude of a star that is induced by the refraction of the earth atmosphere is in a simple model of a flat earth (Green 1985; Filippenko 1982)

$$R \approx (n_0 - 1) \tan z_0, \quad (1)$$

where n_0 is the index of refraction on the ground, z_0 the apparent zenith distance on the ground, and

$$R = z - z_0 > 0 \quad (2)$$

obtained in radian.

This implies chromatic effects (Livengood et al. 1999; Langhans et al. 2003; Colavita et al. 2004; Roe 2002) and dependencies on the atmospheric model, commonly summarized under the label “transversal atmospheric dispersion” in Astronomy. There is a rainbow effect in Eq. (1): as n_0 is a function of the wavelength, R becomes dispersive, too: between wavelengths of $2 \mu\text{m}$ and $2.4 \mu\text{m}$, we get a difference of $\Delta n_0 \approx 1.05 \cdot 10^{-7}$ at 2600 m above sea level, which translates into a spectral smear of $\Delta R \approx 22 \text{ mas} \cdot \tan z_0$.

Eq. (1) suggests that the relative error in the star's altitude definition is close to the relative error in the dielectric function and susceptibility at the telescope site. In addition, Snell's law of refraction states that product $n \sin z$ between the height-dependent index of refraction n and the

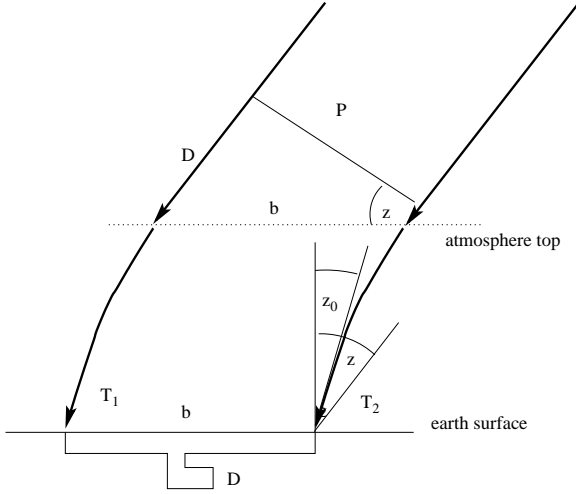


Fig. 1.— The standard model of delay correction and recovery for a star at zenith angle z observed by two telescopes that look through horizontal layers of the stratified atmosphere. $D = b \sin z = P \tan z$.

sine of the angle of refraction at that height remains constant along the path (Green 1985, (4.2)). Therefore the optical path delay is $D = b \sin z = b n_0 \sin z_0$; it changes as the astronomical object changes position in z , or, supposed b is fixed, according to atmospheric parameters accessible at the ground level. The benefit of this analysis is that both, the pointing correction R in Eq. (1) and the OPD measured on the ground, are functions of the index of refraction at the telescope site, not functionals of the entire layered atmosphere.

The theme of this paper are corrections to these statements considering a non-turbulent atmosphere covering an earth surface of constant, but non-negligible curvature. The rest of Sec. 1 shortly describes the standard theory of refraction and defines two different baseline lengths. Sec. 2 concentrates on the integral formulation of the OPD calculation through the atmosphere: geometries with constrained azimuths suffice to introduce all relevant concepts; general star positions are then reduced to the constrained case.

1.2. Spherical Earth: Geometry

Things are more complicated if we start to look at the more realistic model of a spherical earth. A telescope distance of $b = 100$ m on an earth of ra-

dius $\rho = 6368$ km leads to a pointing mismatch of purely geometric origin of about $b/\rho \approx 3.2$ arcsec (Fig. 2). The baseline b is the distance between

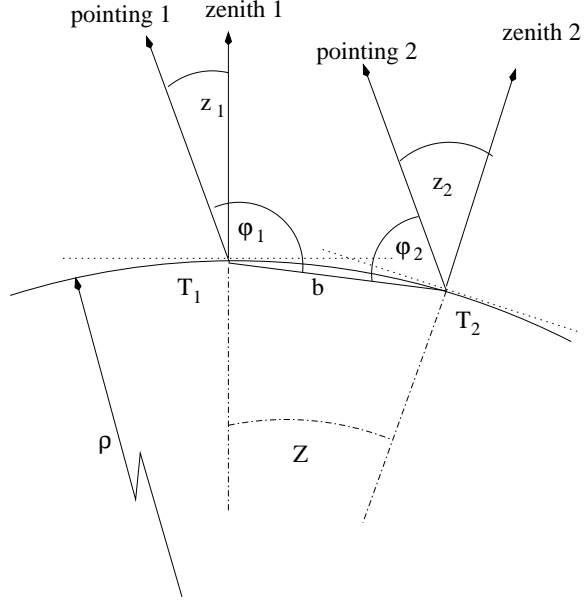


Fig. 2.— Two telescopes placed on the earth of radius ρ at a distance b looking at the same star experience local zenith angles that differ by $Z \approx b/\rho$ rad.

the telescope locations on the earth, the length of the straight secant drawn in Figs. 2 and 3,

$$b = \rho \sqrt{2(1 - \cos Z)} \quad (3)$$

$$= 2\rho \sin \frac{Z}{2} \quad (4)$$

$$\approx \rho \left(Z - \frac{Z^3}{24} + \frac{Z^5}{1920} \dots \right). \quad (5)$$

The inversion of this series reads

$$Z \approx \frac{b}{\rho} + \frac{1}{24} \left(\frac{b}{\rho} \right)^3 + \frac{3}{640} \left(\frac{b}{\rho} \right)^5 \dots \quad (6)$$

The angle approximation $Z \approx b/\rho$ is an estimate to $b/\rho = 2 \sin(Z/2)$, a limit of a baseline so short that it does not matter whether it is measured along a straight line (as drawn in Fig. 2) or along the circular perimeter. The relative error in this approximation is $\approx Z^2/24$, or $\approx 10^{-11}$ for the example of $b = 100$ m.

Pointing/guiding is a functionality of the individual telescopes: the existence of a nonzero point-

pointing “corrections” that already show up in the single ray case, as discussed next.

Eq. (1) is based on the assumption that the gradient of the refractive index n along the ray path is parallel to a global, constant zenith vector. As the gradient and the zenith vector change in direction along the path through a spherically symmetric atmosphere, and as we assume that n becomes a function of the radial distance to the spherical surface of the earth, the equation becomes more accurately (Green 1985, (4.19))(Thomas & Joseph 1995; Auer & Standish 2000; Nener et al. 2003; Noerdlinger 1999; Tannous & Nigrin 2001)

$$R = \rho n_0 \sin z_0 \int_1^{n_0} \frac{dn}{n(r^2 n^2 - \rho^2 n_0^2 \sin^2 z_0)^{1/2}}, \quad (8)$$

an integral over the refractive index, to start above the atmosphere ($n = 1$) and to end at the telescope position ($n = n_0$), and where $r \geq \rho$ is the distance to the earth center. Its Taylor expansion is commonly written as an expansion in powers of $\tan z_0$ (Stone 1996), the observed quantity,

$$\begin{aligned} R = & \rho n_0 \tan z_0 \int_1^{n_0} \frac{dn}{n^2 r} \\ & + \frac{\rho n_0 \tan^3 z_0}{2} \int_1^{n_0} \frac{\rho^2 n_0^2 - r^2 n^2}{n^4 r^3} dn \\ & + \frac{3\rho n_0 \tan^5 z_0}{8} \int_1^{n_0} \frac{(\rho^2 n_0^2 - r^2 n^2)^2}{n^6 r^5} dn + \dots \end{aligned} \quad (9)$$

The major new aspect is that the pointing direction becomes a functional of the height spectrum of the index n , and the angle of arrival becomes site-dependent (Conan et al. 2000).

Accurate modeling of $n(r)$ is not within the scope of this treatise here and unambitiously discussed in App. A. Tables and graphs to follow use an exponential depletion of the susceptibility

$$\chi = \epsilon - 1 = n^2 - 1 \quad (10)$$

to the vacuum of the universe with a scale height K ,

$$\chi(r) = \chi_0 e^{-(r-\rho)/K}. \quad (11)$$

The explicit parameters are

$$\chi_0 = 4 \cdot 10^{-4}, \quad \rho = 6380\text{km}, \quad K = 10\text{km}, \quad (12)$$

unless otherwise noted, representing a prototypical K-band value at 2600 m above sea level

(Mathar 2004). Within this model, Fig. 4 shows the change in R introduced by switching from the flat earth model,

$$R \xrightarrow{\rho \rightarrow \infty} n_0 \sin z_0 \int_1^{n_0} \frac{dn}{n(n^2 - n_0^2 \sin^2 z_0)^{1/2}}, \quad (13)$$

to the spherical model of the atmosphere.

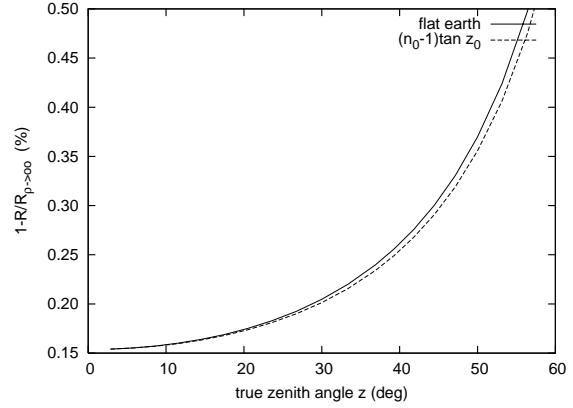


Fig. 4.— Solid line: The relative error in the refraction angle R , in percent, made by switching from the spherical model, Eq. (8), to the limit of the flat earth, Eq. (13). Dashed line: The relative error by switching from the spherical model to the approximation (1). The *absolute* errors approach 0 as $z \rightarrow 0$.

2. Accumulated Optical Path Lengths for Spherical Geometry

2.1. Planar, Overhead Geometry

2.1.1. Single Star

The optical path length along the curved ray trajectory is the line integral of the refractive index over the geometric path, similar to Eq. (8)

$$L = \int_{n=1}^{n_0} n \frac{dr}{\cos \psi}, \quad (14)$$

where $dr/\cos \psi$ is the length of the diagonal path element in Fig. 5. ψ the local zenith angle of the star, and the r the distance from the earth center (Green 1985, Fig. 4.4). This quantity includes the geometric path length up to the star and is infinite in our applications. We assume a maximum height H of the atmosphere, $n|_{r>\rho+H} = 1$,

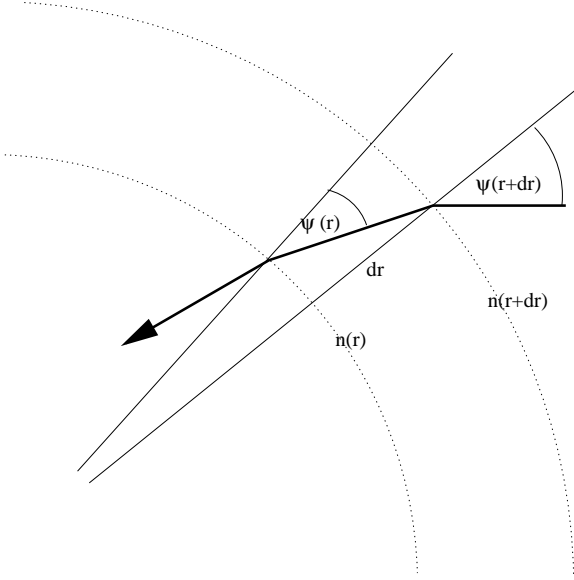


Fig. 5.— The integrals (8) and (14) accumulate the change in the geocentric zenith angle $\psi(r)$ and the optical path length $n/\cos\psi$, respectively, along the light path, applying Snell's law $rn\sin\psi(r) = \text{const}$ at each differential layer.

with the option to look at the limit $H \rightarrow \infty$ if the density has no clear ceiling, like in the models of Eq. (11). We define the impact parameters I_1 and I_2 of the rays, $0 \leq I_2 \leq I_1 \leq \rho$, which were their smallest distances to the earth center if they would pass by along geometric straight lines without any diffraction—as used in atomic collision theory.

$$P = I_1 - I_2 \quad (15)$$

is the projected baseline, measured above the atmosphere. Sec. 2.1 considers the case in which the star, the two telescopes (the baseline), and the earth center are coplanar: Fig. 6. Comments on the general configuration of an unconstrained star azimuth follow in Sec. 2.2.

The difference between the integrals Eq. (14)

$$\begin{aligned} D &= L_1 - L_2 \\ &= \int_{r=\rho}^{\sqrt{(\rho+H)^2 + I_1^2 - I_2^2}} \frac{n dr}{\cos\psi^{(1)}} - \int_{r=\rho}^{\rho+H} \frac{n dr}{\cos\psi^{(2)}} \end{aligned} \quad (17)$$

is the OPD for two telescopes at a common baseline b , with different apparent and different true

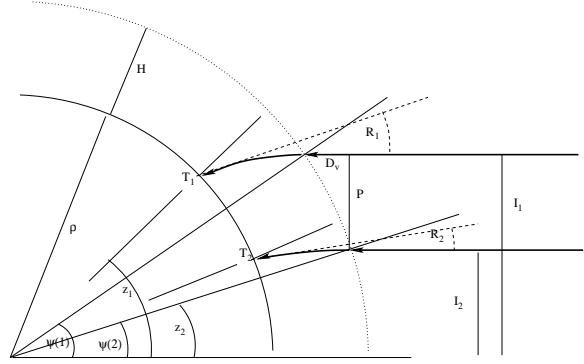


Fig. 6.— Sketch of the impact parameters I_i , the auxiliary geocentric zenith angles $\psi_H^{(i)}$, the true zenith angles z_i , the angles of refraction R_i , and the projected baseline P . The two light rays enter from the right, hit the upper atmosphere at a height H where indicated by the dotted quarter-circle, and eventually the telescopes T_i .

zenith angles (individual pointing), but looking at the same star. The additional straight line segment for the ray to telescope 1 through vacuum before it reaches the altitude H is

$$\begin{aligned} D_v &\equiv \sqrt{(\rho+H)^2 - I_2^2} - \sqrt{(\rho+H)^2 - I_1^2} \\ &= (\rho+H)[\cos\psi_H^{(2)} - \cos\psi_H^{(1)}]. \end{aligned} \quad (18)$$

The Taylor series of this term up to third order in P is

$$D_v \approx P \tan\psi_H^{(2)} + \frac{1}{2I_2} \frac{\tan\psi_H^{(2)}}{\cos^2\psi_H^{(2)}} P^2 + \frac{1}{2I_2^2} \frac{\tan^3\psi_H^{(2)}}{\cos^2\psi_H^{(2)}} P^3. \quad (19)$$

We separate this piece from the integral for the telescope 1,

$$D = D_v + \int_{r=\rho}^{\rho+H} n \left[\frac{1}{\cos\psi^{(1)}} - \frac{1}{\cos\psi^{(2)}} \right] dr, \quad (20)$$

where the major difference w.r.t. Fig. 1 is that this integral does not vanish, because the atmosphere is now hit at two different angles $\psi_H^{(1)} \neq \psi_H^{(2)}$. The integral would also not vanish, if the factor n would be dropped to deduce the *geometric* path difference of the curved beams.

The constance of the product $rn\sin\psi$ along each curved trajectory (Green 1985, (4.16)),

$$rn\sin\psi^{(1)} = (\rho+H)\sin\psi_H^{(1)} = I_1; \quad (21)$$

$$rn\sin\psi^{(2)} = (\rho+H)\sin\psi_H^{(2)} = I_2, \quad (22)$$

is inserted into the previous equation,

$$D = D_v + \int_{r=\rho}^{\rho+H} r n^2 \left[\frac{1}{\sqrt{r^2 n^2 - (\rho + H)^2 \sin^2 \psi_H^{(1)}}} - \frac{1}{\sqrt{r^2 n^2 - (\rho + H)^2 \sin^2 \psi_H^{(2)}}} \right] dr \quad (23)$$

The term in square brackets allows another Taylor expansion

$$\begin{aligned} \frac{1}{\sqrt{r^2 n^2 - I_1^2}} - \frac{1}{\sqrt{r^2 n^2 - I_2^2}} &\approx \\ \frac{I_2}{(r^2 n^2 - I_2^2)^{3/2}} P + \frac{1}{2} \frac{r^2 n^2 + 2I_2^2}{(r^2 n^2 - I_2^2)^{5/2}} P^2 \\ + \frac{1}{2} \frac{3r^2 n^2 + 2I_2^2}{(r^2 n^2 - I_2^2)^{7/2}} I_2 P^3. \end{aligned} \quad (24)$$

All correction terms of the spherical geometry in Eqs. (19)–(24) have a positive sign. The contribution of the term of $O(P^2)$ amounts to ≈ 2 mm, and of the term of $O(P^3)$ to ≈ 60 nm as the zenith angle approaches 60 deg at $b = 100$ m. A consistency check of Eq. (24) is that its contribution of the first, linear Taylor order to the integral in Eq. (23) becomes

$$\begin{aligned} \int_{r=\rho}^{\rho+H} r n^2 \frac{I_2 P}{(r^2 n^2 - I_2^2)^{3/2}} dr \\ \xrightarrow{n \rightarrow 1} -P \tan \psi_H^{(2)} + P \frac{I_2}{\sqrt{\rho^2 - I_2^2}} \end{aligned} \quad (25)$$

in the vacuum limit, such that the term $P \tan \psi_H^{(2)}$ cancels the first term in Eq. (19), and only the term $P \tan z$ depending on the true topocentric zenith angle remains, equivalent to Fig. 1.

The influence of the spherical geometry on the atmospheric path length difference is demonstrated in Fig. 7.

2.1.2. Astrometry (two true zenith distances)

Up to here, an accurate computation of the delay D by integration over the atmosphere layers is not competitive against measuring the equivalent value on the ground (Fig. 1), since the gas densities on the ground along the beam path—input to calculation of the refractive indexes—are accessible to sensors and much better known than

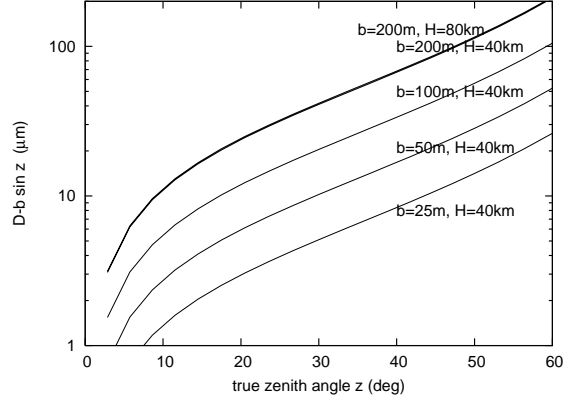


Fig. 7.— The difference between the full integral (23) of the delay D and the approximation $D \approx b \sin \bar{z}$, which one would derive from Fig. 1 using the mean true zenith angle $\bar{z} \equiv (z_1 + z_2)/2$, for baselines between 25 and 200 m. A convergence test to the limit $H \rightarrow \infty$ is indicated for $b = 200$ m.

the remote, high-flying layers of air. As we turn to the astrometric task of completing the right-angled triangle formed by D , P and b^* in Fig. 3—with the aim of precise determination of either of the base angles at b^* —, the “baseline calibration” emerges as an additional focus. This means determination of b^* , the image of b . The following sections consider the atmospheric lensing correction $b^* - b$ to a, in principle, rock-solid and accessible ground baseline b . The computational strategy is to derive P and D , then to use Eq. (7). Within this framework, the geometric baseline b is defined joining the “ends of the paths through the atmosphere,” and is assumed to be the same vector for both stars in the case of astrometry. We do not ask the question whether the corresponding terminal points T_1 and T_2 are that well defined for real telescope optics with chromatic, azimuth dependent foci and trusses that bent under the load of their own weight or the wind.

The formal solution to the problem of tracing four beams (two stars, separated by an angle τ and labeled P for “primary” and S for “secondary,” to two telescopes) for a given Z in Eq. (6) is then given by computation of D_P for the primary at some Z (some baseline b , see Eq. (5)), computation of D_S for the secondary at the same $\Delta z = Z = z_{1S} - z_{2S} = z_{1P} - z_{2P}$ (since the secondary must

be caught by the same two telescopes) but slightly different true zenith angles $z_1S = z_1P + \tau$, $z_2S = z_2P + \tau$. It should be noted that the earth-bound baseline is *not* tilted here— there is no lifting of one telescope and sinking of the other to acquire the secondary—, and b refers to the geometrical distance between two foci that define a common reference for both stars. Any residual effects of the spherical atmosphere and/or atmospheric layering are then caused by the second derivative of $L(z)$ (Fig. 8).

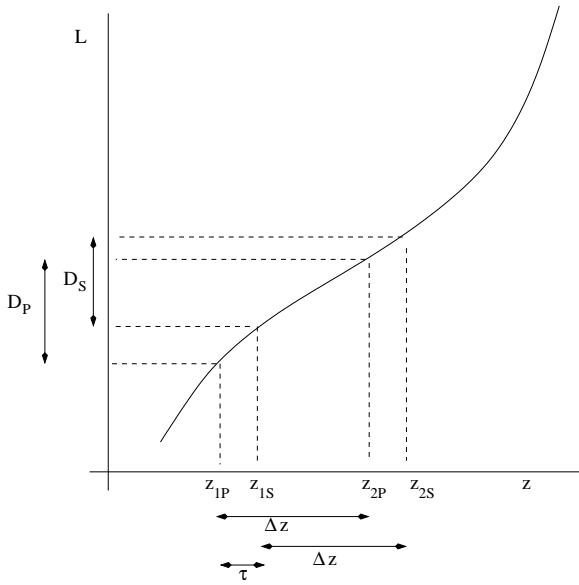


Fig. 8.— A difference in the delays D_P and D_S measured for the primary star and the secondary star is caused by the nonlinearity of the path length L , Eq. (14), as a function of the true zenith position.

From (23) with (22), omitting a constant $\rho + H$,

$$L = -\sqrt{(\rho + H)^2 - \rho^2 n_0^2 \sin^2 z_0} + \int_{r=\rho}^{\rho+H} \frac{r n^2}{(r^2 n^2 - \rho^2 n_0^2 \sin^2 z_0)^{1/2}} dr, \quad (26)$$

where we insert $z_0 = z - R$. For a spherical earth without atmosphere, the vacuum limit,

$$R \xrightarrow{n \rightarrow 1} 0, \quad n_0 \rightarrow 1, \quad (27)$$

$$\begin{aligned} L &\longrightarrow \rho(1 - \cos z) \\ &= \frac{\rho}{2} \tan^2 z - \frac{3}{8} \rho \tan^4 z + \frac{5}{16} \rho \tan^6 z. \end{aligned} \quad (28)$$

$$D \longrightarrow \rho(\cos z_2 - \cos z_1). \quad (29)$$

This suggests we define an effective true zenith angle \bar{z} via

$$D \equiv b \sin \bar{z} = P \tan \bar{z}, \quad (30)$$

and use Eqs. (5) and (29) to prove that this equals the mean,

$$\bar{z} = \frac{z_1 + z_2}{2}. \quad (31)$$

Since the astrometric signature is hidden in the second derivative of $L(z)$, the computationally most appealing expansion of R and L is a Taylor series around some reference value of z :

$$R|_{z+x} \equiv \xi_0 + \xi_1 x + \xi_2 x^2 + \xi_3 x^3 + \dots, \quad \xi_0 = R|_z. \quad (32)$$

We define refractivity integrals as a short-cut to the notation, covering Eq. (8) as a special case:

$$R_j \equiv I^{2j+1} \int_1^{n_0} \frac{dn}{n(r^2 n^2 - I^2)^{j+1/2}}, \quad (33)$$

$$I \equiv \rho n_0 \sin z_0, \quad j = 0, 1, 2, \dots \quad (34)$$

A stable numerical scheme for these integrals is proposed in App. B. Insertion of the series (32) into the l.h.s. of (8) and into the arguments $z_0 = z - R$ of the sines at the r.h.s. yields the expansion coefficients

$$\xi_0 = R_0, \quad (35)$$

$$\xi_1 = \frac{R_0 + R_1}{\tan z_0} / \left(1 + \frac{R_0 + R_1}{\tan z_0} \right), \quad (36)$$

$$\begin{aligned} \xi_2 &= \frac{(\xi_1 - 1)^3}{2} \left[R_0 + R_1 - 3 \frac{R_1 + R_2}{\tan^2 z_0} \right] \\ &= \frac{[3R_{12} - R_{01} \tan^2 z_0] \tan z_0}{2\hat{R}_{01}^3}, \end{aligned} \quad (37)$$

$$\begin{aligned} \xi_3 &= -(\xi_1 - 1)^2 \left[-(R_0 + R_1)\xi_2 + 3 \frac{R_1 + R_2}{\tan^2 z_0} \xi_2 \right. \\ &\quad \left. + \frac{(\xi_1 - 1)^2}{\tan z_0} \left\{ \frac{1}{6} R_0 + \frac{5}{3} R_1 - 3 \frac{R_2}{\tan^2 z_0} \right. \right. \\ &\quad \left. \left. - \frac{1}{2} \frac{R_1}{\tan^2 z_0} - \frac{5}{2} \frac{R_3}{\tan^2 z_0} + \frac{3}{2} R_2 \right\} \right] \\ &= -\frac{\tan z_0}{6\hat{R}_{01}^5} \left[15(R_1 - R_3)\hat{R}_{01} \right. \\ &\quad \left. + 9R_{12}(3R_{12} - 2\hat{R}_{01} - \bar{R}_{01} \tan^2 z_0) \right. \\ &\quad \left. + R_{01}(\hat{R}_{01} + 3R_{01} \tan^2 z_0) \tan^2 z_0 \right], \end{aligned} \quad (38)$$

$$\begin{aligned} &= -\frac{\tan z_0}{6\hat{R}_{01}^5} \left[15(R_1 - R_3)\hat{R}_{01} \right. \\ &\quad \left. + 9R_{12}(3R_{12} - 2\hat{R}_{01} - \bar{R}_{01} \tan^2 z_0) \right. \\ &\quad \left. + R_{01}(\hat{R}_{01} + 3R_{01} \tan^2 z_0) \tan^2 z_0 \right], \end{aligned} \quad (39)$$

with the doubly-indexed shorthands

$$R_{ij} \equiv R_i + R_j, \quad (40)$$

$$\hat{R}_{ij} \equiv R_i + R_j + \tan z_0, \quad (41)$$

$$\bar{R}_{ij} \equiv R_i + R_j - \tan z_0. \quad (42)$$

In Eqs. (33)–(42) and App. B, the subscripts of R are the exponential j of the definition (33); elsewhere they indicate the telescope number/site. x

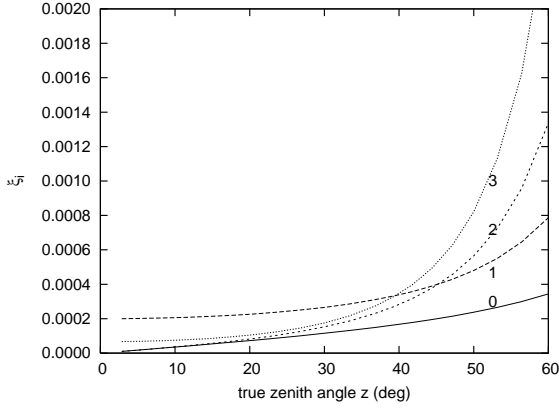


Fig. 9.— The expansion coefficients ξ_j of Eq. (32) as a function of zenith angle z for $j = 0, \dots, 3$ and the atmospheric model (11)–(12). R is an odd function of z , so the even-indexed ξ_j approach 0 for $z \rightarrow 0$. ξ_1 approaches $n_0 - 1$, see Eq. (1).

in Eq. (32) is of the order of $b/(2\rho)$ if the reference azimuth z is chosen close to the middle between the telescopes, and therefore not larger than $1.6 \cdot 10^{-5}$ rad for $b < 200$ m. Because the ξ_j are approximately of the same magnitude (Fig. 9), collecting the terms up to $j = 3$ ought establish a relative accuracy of $\approx 5 \cdot 10^{-14}$ in the angle of refraction.

The expansion

$$L_{|z+x} = L_{|z} + \sum_{i=1,2,3,\dots} l_i x^i, \quad (43)$$

proceeds via insertion of Eq. (32) into the sines of Eq. (26), and employs an auxiliary set of integrals

$$v_i \equiv I^{2i} \left[\frac{1}{[(\rho + H)^2 - I^2]^{i-1/2}} + (2i-1) \int_{r=\rho}^{\rho+H} \frac{r n^2}{(r^2 n^2 - I^2)^{i+1/2}} dr \right] \xrightarrow{n \rightarrow 1, I \rightarrow \rho \sin z} \rho \tan^{2i} z \cos z. \quad (44)$$

$$l_1 = \frac{1 - \xi_1}{\tan z_0} v_1 \xrightarrow{n \rightarrow 1, I \rightarrow \rho \sin z} \rho \sin z, \quad (45)$$

$$l_2 = -\frac{1}{2} v_1 \left[\left(1 - \frac{1}{\tan^2 z_0}\right) (1 - \xi_1)^2 + \frac{2\xi_2}{\tan z_0} \right] + \frac{1}{2} v_2 \frac{(1 - \xi_1)^2}{\tan^2 z_0} \quad (46)$$

$$\xrightarrow{n \rightarrow 1, I \rightarrow \rho \sin z} \frac{1}{2} \rho \cos z, \quad (47)$$

$$l_3 = \frac{1}{3} v_1 (1 - \xi_1) \left[-2 \frac{(1 - \xi_1)^2}{\tan z_0} + 3\xi_2 \left(1 - \frac{1}{\tan^2 z_0}\right) \right] - \frac{1}{2} v_2 \frac{1 - \xi_1}{\tan z_0} \left[\left(1 - \frac{1}{\tan^2 z_0}\right) (1 - \xi_1)^2 + \frac{2\xi_2}{\tan z_0} \right] + \frac{1}{2} v_3 \frac{(1 - \xi_1)^3}{\tan^3 z_0} \xrightarrow{n \rightarrow 1, I \rightarrow \rho \sin z} -\frac{1}{6} \rho \sin z,$$

$$l_4 \xrightarrow{n \rightarrow 1, I \rightarrow \rho \sin z} -\frac{1}{24} \rho \cos z. \quad (48)$$

If the l_i are calculated at the mean position

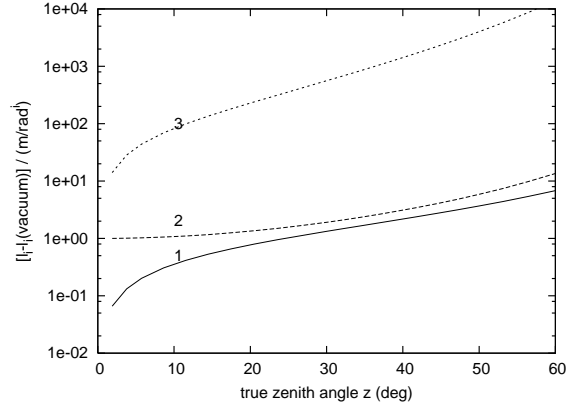


Fig. 10.— The differences between the Taylor expansion coefficients l_j of Eq. (43) and their vacuum values as a function of zenith angle z for $j = 1, \dots, 3$, parametrized through the exponential model (11)–(12). L is an even function of z , so the odd-indexed l_j approach 0 for $z \rightarrow 0$. The vacuum limits, Eq. (29), are $l_1 \rightarrow \rho \sin z$, $l_2 \rightarrow \rho(\cos z)/2$, $l_3 \rightarrow -\rho(\sin z)/6$.

$\bar{z} = (z_1 + z_2)/2$, the delay for a single sky position becomes

$$D \approx l_1 (z_1 - z_2) + l_2 (z_1^2 - z_2^2) + l_3 (z_1^3 - z_2^3) + l_4 (z_1^4 - z_2^4) + \dots \quad (49)$$

$$\approx l_1 \Delta z + l_3 (\Delta z)^3 / 4 + l_5 (\Delta z)^5 / 16 + l_7 (\Delta z)^7 / 64 + \dots \quad (50)$$

If the l_i are calculated at the mean position $\bar{z} = (z_{1P} + z_{2P})/2$, the differential delay is to lowest orders in τ

$$\begin{aligned} D_S - D_P &= \Delta z \tau \left[2l_2 + 3\tau l_3 + ((\Delta z)^2 + 4\tau^2) l_4 \right. \\ &\quad + \left(\frac{5}{2} (\Delta z)^2 \tau + 5\tau^3 \right) l_5 \\ &\quad \left. + \left(\frac{3}{8} (\Delta z)^4 + 5(\Delta z)^2 \tau^2 + 6\tau^4 \right) l_6 + \dots \right] \end{aligned} \quad (51)$$

The leading term $2\Delta z \tau l_2$ contains

- the familiar geometric “vacuum” contribution $\Delta z \rho \tau \cos z \approx b \tau \cos z$; see Eqs. (6) and (47),
- an atmospheric correction to l_2 of the order of 1–10 m/rad² (Fig. 10). It adds some tens of nanometers to the differential delay, if $\tau < 1$ arcmin = $3 \cdot 10^{-4}$ rad, and $\Delta z < 3 \cdot 10^{-5}$ rad ($b < 200$ m). There is no equivalent contribution of this kind in planar earth models like Fig. 1.

With Eqs. (15) and (32),

$$I_1 = \rho n_0 \sin(z_1 - R_1) \quad (52)$$

$$\approx \rho n_0 \sin \left(\bar{z} - \xi_0 + (1 - \xi_1) \frac{\Delta z}{2} - \xi_2 \frac{(\Delta z)^2}{4} - \xi_3 \frac{(\Delta z)^3}{8} - \dots \right), \quad (53)$$

$$I_2 = \rho n_0 \sin(z_2 - R_2) \quad (54)$$

$$\approx \rho n_0 \sin \left(\bar{z} - \xi_0 + (\xi_1 - 1) \frac{\Delta z}{2} - \xi_2 \frac{(\Delta z)^2}{4} + \xi_3 \frac{(\Delta z)^3}{8} - \dots \right), \quad (55)$$

we may expand P^2 in a power series of Δz ,

$$\begin{aligned} P^2 &\approx \{ \rho n_0 \cos \bar{z}_0 (1 - \xi_1) \}^2 (\Delta z)^2 \\ &\quad + \frac{1}{12} \rho^2 n_0^2 \cos \bar{z}_0 (1 - \xi_1) \\ &\quad \times \{ [(\xi_1 - 1)^3 - 6\xi_3] \cos \bar{z}_0 + 6\xi_2 [1 - \xi_1] \sin \bar{z}_0 \} \\ &\quad \times (\Delta z)^4 + \dots \end{aligned} \quad (56)$$

We do the same for D^2 via Eq. (50), and eventually combine these power series of Δz at the r.h.s. of Eq. (7),

$$b^{*2} \approx \left\{ (1 - \xi_1)^2 \rho^2 n_0^2 \cos^2 \bar{z}_0 + l_1^2 \right\} (\Delta z)^2$$

$$\begin{aligned} &+ \left\{ \frac{\rho^2 n_0^2 (1 - \xi_1) \cos \bar{z}_0}{12} \left([(\xi_1 - 1)^3 - 6\xi_3] \cos \bar{z}_0 \right. \right. \\ &\quad \left. \left. + 6\xi_2 [1 - \xi_1] \sin \bar{z}_0 \right) + \frac{l_1 l_3}{2} \right\} (\Delta z)^4 \\ &+ \dots \end{aligned} \quad (57)$$

which turns into Eq. (5) in the vacuum limit. Examples of this “baseline magnification” introduced by the atmosphere are shown in Fig. 11; the effect becomes larger if the transition into the free space is smoothed by choosing a large cut-off height H .

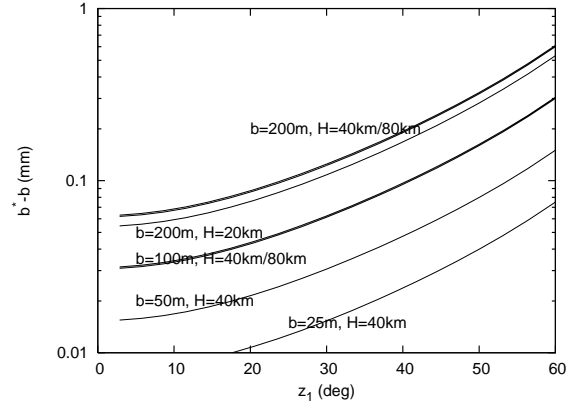


Fig. 11.— The difference $b^* - b$ between the length of the effective baseline above the atmosphere and the geometric baseline on the ground according to Eq. (57) as a function of z_1 , parametrized through the model (11)–(12), which is cut off at $H = 20, 40$ or 80 km.

2.2. 3D Geometry

2.2.1. Geographic Coordinates

The previous section dealt with the case where the telescopes, the star and the earth center are coplanar. In the general case, the direction of the star and the direction of the second telescope do not share the same azimuth A . Let the telescopes have geographical latitudes Φ_i and longitudes λ_i in a geocentric spherical coordinate system:

$$\mathbf{r}_i = \rho \begin{pmatrix} \cos \lambda_i \cos \Phi_i \\ \sin \lambda_i \cos \Phi_i \\ \sin \Phi_i \end{pmatrix}, \quad (i = 1, 2). \quad (58)$$

For the Very Large Telescope Interferometer in Northern Chile $\Phi \approx -0.4298$ rad and $\lambda \approx -1.229$

rad, for instance. The baseline angle in Eq. (3) becomes

$$\cos Z = \sin \Phi_1 \sin \Phi_2 + \cos \Phi_1 \cos \Phi_2 \cos(\Delta\lambda), \quad (59)$$

where $\Delta\lambda \equiv \lambda_1 - \lambda_2$. To transform Cartesian coordinates from the local alt-az-system of telescope i (with the Cartesian coordinate z pointing to the zenith, x horizontally tangentially to the earth toward north and the local horizon as indicated by the dotted line in Fig. 2, y horizontally toward west) to the geocentric system (with z pointing from the earth center to the north pole, x from the center to the equator south of Greenwich, y from the center to the equator 1000 km west of Sumatra) we translate the coordinates into a tilted system originating from the earth center, then (de)rotate them:

$$\mathbf{r}_c = \begin{pmatrix} -\sin \Phi_i \cos \lambda_i & \sin \lambda_i & \cos \Phi_i \cos \lambda_i \\ -\sin \Phi_i \sin \lambda_i & -\cos \lambda_i & \cos \Phi_i \sin \lambda_i \\ \cos \Phi_i & 0 & \sin \Phi_i \end{pmatrix} \cdot \left(\mathbf{r}_i + \begin{pmatrix} 0 \\ 0 \\ \rho \end{pmatrix} \right), \quad i = 1, 2. \quad (60)$$

The inverse operation with the inverse matrix (which equals the transpose matrix) is

$$\mathbf{r}_i = \begin{pmatrix} -\sin \Phi_i \cos \lambda_i & -\sin \Phi_i \sin \lambda_i & \cos \Phi_i \\ \sin \lambda_i & -\cos \lambda_i & 0 \\ \cos \Phi_i \cos \lambda_i & \cos \Phi_i \sin \lambda_i & \sin \Phi_i \end{pmatrix} \cdot \mathbf{r}_c - \begin{pmatrix} 0 \\ 0 \\ \rho \end{pmatrix}. \quad (61)$$

The product of two such operations with indexes 1 and 2 converts the two alt-az systems: starting in Eq. (60) with $\mathbf{r}_2 = 0$, computing \mathbf{r}_c , and inserting this into (61) for $i = 1$ shows that the origin of coordinates of telescope 2 is located at

$$\mathbf{b}_{12} = \rho \cdot \begin{pmatrix} -\sin \Phi_1 \cos \Phi_2 \cos(\Delta\lambda) + \cos \Phi_1 \sin \Phi_2 \\ \cos \Phi_2 \sin(\Delta\lambda) \\ \cos \Phi_1 \cos \Phi_2 \cos(\Delta\lambda) + \sin \Phi_1 \sin \Phi_2 - 1 \end{pmatrix}$$

seen from the origin of telescope 1. The length of this vector is $b = |\mathbf{b}_{12}|$ of Eq. (3), using Eq. (59); the third coordinate is negative since the second telescope lies below the horizon of the first telescope (and vice versa), as illustrated in Fig. 2.

2.2.2. Vacuum limit

If the atmosphere is absent, the star direction is defined as

$$\mathbf{s}_i = \begin{pmatrix} \cos A_i \sin z_i \\ \sin A_i \sin z_i \\ \cos z_i \end{pmatrix}, \quad i = 1, 2, \quad (62)$$

in terms of the true local azimuth A_i and true zenith angle z_i in the i th telescope coordinate system. A is counted positive starting from N to W. [This azimuth convention is the one of (Smart 1949, §II); the alternative convention of (Taff 1980; Karttunen et al. 1987) is obtained with the replacement $A_i \rightarrow \pi - A_i$.] The cosine of the angle between the star and the baseline in Fig. 2 is

$$\cos \varphi_1 = \mathbf{s}_1 \cdot \mathbf{b}_{12}/b, \quad (63)$$

where $\mathbf{s}_1 \cdot \mathbf{b}_{12}$ is known as the geometric optical path delay. If one swaps the indexes 1 and 2, the cosine switches its sign, because in this parallax-free situation the angle between star and baseline is the 180°-complement of the angle relative to the other telescope:

$$\cos \varphi_2 = \mathbf{s}_2 \cdot \mathbf{b}_{21}/b = -\cos \varphi_1. \quad (64)$$

This may be verified with the standard coordinate transformations between the hour angles h_i and right ascension δ for $i = 1, 2$,

$$\cos \delta \sin h_i = \sin z_i \sin A_i, \quad (65)$$

$$\sin z_i \cos A_i = \cos \Phi_i \sin \delta - \sin \Phi_i \cos \delta \cos h_i, \quad (66)$$

$$\cos z_i = \sin \Phi_i \sin \delta + \cos \Phi_i \cos \delta \cos h_i, \quad (67)$$

$$h_1 - h_2 = \lambda_1 - \lambda_2 \quad (68)$$

So if the atmosphere is absent, this angle relates to $P = |\sin \varphi_i|b$ ($i = 1, 2$) as shown in Fig. 3.

The mean and difference in the true zenith angles remain defined as in Eqs. (31) and

$$\Delta z \equiv z_1 - z_2, \quad (69)$$

and can be retrieved from the geographical coordinates (66)–(67) and (Abramowitz & Stegun 1972, (4.3.34)–(4.3.37)).

2.2.3. Ray tracing

There is one distinguished geocentric coordinate system for the case of a single star, shown in Fig. 12, in which the direction vectors of the incoming light above the atmosphere have only a component along the polar axis. The side view of this geometry reduces to Fig. 6 if the positions 1, 1v, 2 and 2v lie on the same projected straight line. (In the following, “projected” means projected onto a plane perpendicular to the ray propagation above the atmosphere.) The strat-

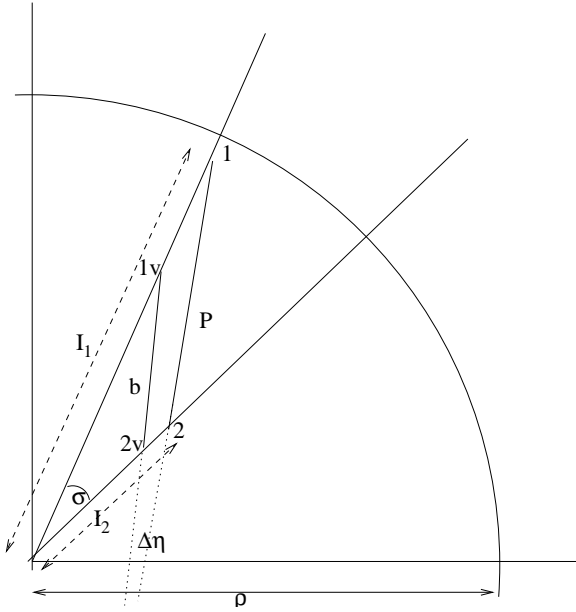


Fig. 12.— A top view of the earth coordinates as seen from the incoming two rays in which both \mathbf{s}_i are perpendicular to the plane of the drawing. If the atmosphere were absent, the first ray would see telescope 1 at the position 1v. The atmospheric refraction pulls rays toward the earth center, which means it has to relocate its impact at the top of the atmosphere to the actual image position 1 above the atmosphere to end up at telescope 1 on the ground. The same effect for ray 2 means the projected baseline vector P above the atmosphere from 1 to 2 is both longer and tilted by $\Delta\eta$ compared to the vacuum case from 1v to 2v.

egy to transform the star position to the projected baseline (vector) P is (i) to calculate the triangle formed by the vacuum baseline and the earth

center seen by the incoming light, and (ii) stretch this radially outward to include the effect of the two difference refraction angles R_i : the two true zenith angles z_i for both telescopes are assumed to be given via Eq. (67). The impact parameters I_i of the rays for the vacuum case are $\rho \sin z_i$ and they equal the lengths of the (projected) station vectors from the earth center to the points 1v and 2v in Fig. 12. The vacuum baseline in Fig. 12 stretches from 1v to 2v, which has the projected length $b|\sin \varphi_i|$ as written down in Eq. (63). The projected baseline aperture angle σ in the triangle with side lengths $\rho \sin z_i$ and $b|\sin \varphi_i|$ relates to the impact parameters and projected vacuum baseline by planar trigonometry (Abramowitz & Stegun 1972, 4.3.148),

$$\sin^2 z_1 + \sin^2 z_2 = 2 \sin z_1 \sin z_2 \cos \sigma + \frac{b^2}{\rho^2} \sin^2 \varphi_1. \quad (70)$$

σ is the projection of Z defined in Eq. (59). The equation mingles the true zenith angles from the two telescope's point of view with the angles φ_i , which represent the star distance from the baseline direction. One may reduce this to the geographic coordinates by multiplying $\mathbf{r}_1 + \mathbf{b}_{12} = \mathbf{r}_2$ with \mathbf{s}_1 to get

$$\cos \sigma = \frac{\cos Z - \cos z_1 \cos z_2}{\sin z_1 \sin z_2} \quad (71)$$

$$= 1 - \frac{\cos(z_1 - z_2) - \cos Z}{\sin z_1 \sin z_2}. \quad (72)$$

$\cos \sigma$ and $\cos Z$ are close to unity in contemporary optical interferometry, so the actual implementation avoids the use of the cosine in favor of the haversine,

$$\text{hav } \sigma = \frac{\sin \frac{Z+\Delta z}{2} \sin \frac{Z-\Delta z}{2}}{\sin z_1 \sin z_2} \quad (73)$$

$$\begin{aligned} &= \frac{Z^2 - (\Delta z)^2}{4 \sin^2 \bar{z}} - \left(\frac{1}{16} - \frac{1}{48} \sin^2 \bar{z} \right) \left(\frac{\Delta z}{\sin \bar{z}} \right)^4 \\ &\quad - \frac{1}{48} \left(\frac{Z}{\sin \bar{z}} \right)^4 + \frac{1}{16} \frac{Z^2 (\Delta z)^2}{\sin^4 \bar{z}} \\ &\quad - (45 - 30 \sin^2 \bar{z} + 2 \sin^4 \bar{z}) \frac{(\Delta z)^6}{2880 \sin^6 \bar{z}} \\ &\quad + (3 - \sin^2 \bar{z}) \frac{(\Delta z)^4 Z^2}{192 \sin^6 \bar{z}} - \frac{(\Delta z)^2 Z^4}{192 \sin^4 \bar{z}} \\ &\quad + \frac{Z^6}{1440 \sin^2 \bar{z}} + \dots, \end{aligned} \quad (74)$$

to protect against cancellation of significant digits, and returns from there to the sine, if needed,

$$\begin{aligned} \sin \sigma &= 2\sqrt{\text{hav } \sigma}\sqrt{1 - \text{hav } \sigma} \\ &= 2\sqrt{\text{hav } \sigma} \left[1 - \sum_{j=1}^{\infty} \frac{(2j-3)!!}{j!} \left(\frac{\text{hav } \sigma}{2} \right)^j \right] \\ &= \sqrt{\text{hav } \sigma} \left(2 - \text{hav } \sigma - \frac{\text{hav}^2 \sigma}{4} - \frac{\text{hav}^3 \sigma}{8} \dots \right). \end{aligned} \quad (75)$$

The special coplanar case of Sec. 2.1 is included as $\Delta z = Z$ and $\sigma = 0$ or π . (On some Linux systems, where the `cosl` library function does not support the full accuracy of the 96 bit `long double` number representation, it makes sense to switch to alternative high-precision implementations of the cosine (Schonfelder 1980).) Two calculations for the actual impact parameters $I_i = \rho n_0 \sin z_0^{(i)}$ starting from the given z_i would be done as in the preceding, “aligned” geometry of Sec. 2.1, and these inserted into

$$I_1^2 + I_2^2 = 2I_1 I_2 \cos \sigma + P^2 \quad (76)$$

to calculate the projected baseline P and to generalize Eq. (15). $P^2 = (I_1 - I_2)^2 + 4I_1 I_2 \text{hav } \sigma$ comprises the terms of Eq. (56) of the constrained geometry augmented by

$$4I_1 I_2 \text{hav } \sigma = (\rho n_0 \sin \bar{z}_0)^2 \frac{Z^2 - (\Delta z)^2}{\sin^2 \bar{z}} + \dots \quad (77)$$

as read from Eq. (74) in combination with Eqs. (53)–(55).

To calculate the path difference $D = L_1 - L_2$ between the two rays above the atmosphere, Eq. (18) remains valid, but in general a Taylor expansion akin to (19) does not exist, because $P \geq I_i \sin \sigma$ ($i = 1, 2$) excludes small P at arbitrary σ . Eq. (32) remains in use to expand the refraction angle in a neighborhood of \bar{z} , and so do Eqs. (43)–(50) that depend only on zenith distances but not on azimuths.

2.2.4. Baseline Rotation

The rotation angle between the baseline b (projected on a plane perpendicular to the star direction) and P is $\Delta\eta \equiv \eta_P - \eta_b$ where η_b and η_P are the angles from b to I_2 and P to I_2 respectively, and given by

$$\frac{I_2}{I_1} = \cos \sigma + \sin \sigma \cot \eta_P, \quad (78)$$

$$\frac{\sin z_2}{\sin z_1} = \cos \sigma + \sin \sigma \cot \eta_b. \quad (79)$$

Numerical examples are presented in Figs. 13–14: By symmetry, the rotation effect vanishes if the star azimuth is along the baseline or perpendicular to it. The angle $\Delta\eta$ may be about five times larger than the interferometric resolution of a 200 m baseline in the K-band: the interferometric fringes appear slightly rotated on the detector, and the true (u, v) coordinate is found by rotating the “apparent” vector by $-\Delta\eta$.

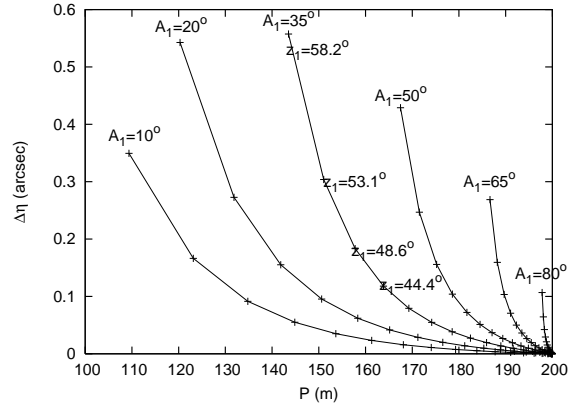


Fig. 13.— The baseline rotation $\Delta\eta$ introduced in Fig. 12 for a baseline $b = 200\text{m}$, for 6 different azimuth angles A_1 measured from T_1 toward the baseline, and for $\sin z_1$ changing in equidistant steps of 0.05 from 0.05 to 0.85.

There is no intrinsically new aspect compared to the analysis of Sec. 2.1: The rotation of the baseline vector P relative to the projection of b would again be absorbed into the pointing direction of the two telescopes. With only one (scalar) observable, which is the differential delay, one cannot measure both the astrometric angle (distance) between two stars and the positioning angle of the S relative to the P at the same time.

2.2.5. Astrometric Case

Eq. (51) obviously loses its meaning because the secondary star now has two degrees of freedom and can no longer be positioned by a single angle τ . The details follow by writing down Eq. (67) for both telescopes and both stars. If the star distances τ_h and τ_δ are defined as

$$h_S \equiv h_P + \tau_h, \quad \delta_S \equiv \delta_P + \tau_\delta, \quad (80)$$

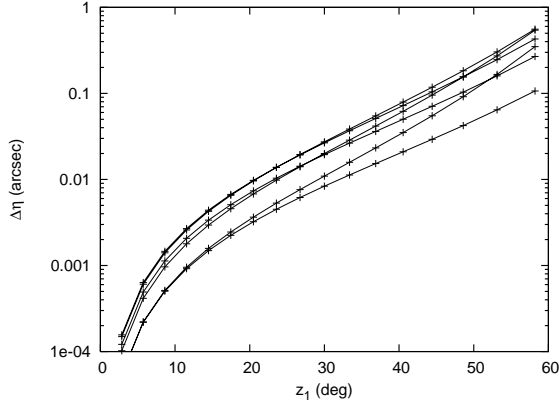


Fig. 14.— An alternative view on the six lines of Fig. 13 with the abscissa switched from the projected baseline length to the azimuth angle. Each small cross has a counterpart in Fig. 13. This graph would not change visibly choosing a baseline of $b = 100$ m.

the expansion of Eq. (67) yields for $z_{iS} \equiv z_{iP} + \tau_{iz}$ to lowest order in τ_h and τ_δ :

$$\begin{aligned} \tau_{iz} = & \frac{\cos \Phi_i \sin \delta_P \cos h_P - \sin \Phi_i \cos \delta_P}{\sin z_{iP}} \tau_\delta \\ & + \frac{\cos \Phi_i \cos \delta_P \sin h_P}{\sin z_{iP}} \tau_h + \dots \end{aligned} \quad (81)$$

The changes τ_{iA} in the azimuths are not detailed here, since the refraction is determined by the zenith angles; they are expected to ensure that the associated change in the star direction (62) forms an acute angle to the baseline to maintain the interferometric resolution. The symmetry suggested in Fig. 8 will generally be broken: $\Delta z_P \neq \Delta z_S$. Restarting from Eq. (50), the differential delay is expanded in powers of the doubly differential $\Delta\tau_z$:

$$\begin{aligned} D_S - D_P &= \Delta z_P \bar{\tau}_z \left[2l_2 + 3\bar{\tau}_z l_3 + ((\Delta z_P)^2 + 4\bar{\tau}_z^2) l_4 \right. \\ &\quad \left. + \dots \right] + O(\Delta\tau_z), \end{aligned} \quad (82)$$

with $\bar{\tau}_z \equiv (\tau_{1z} + \tau_{2z})/2$ and $\Delta\tau_z \equiv \tau_{1z} - \tau_{2z}$, where the l_j are again evaluated at the mean primary zenith, $(z_{1P} + z_{2P})/2$.

3. Summary

The optical path length integral of star light passing through the atmosphere can be handled

with numerical and analytical methods known from treatments of the more familiar refractivity integral. Subtraction of two of these computes the optical path difference, and renormalizes the optical path lengths to start from a common plane tangential to the earth's upper atmosphere, which at the same time defines the projected baseline in this plane perpendicular to the two rays. Definition of a right triangle above the atmosphere with the projected baseline and the path difference as two catheti defines a hypotenuse, which is an effective baseline that is longer than and rotated relative to the geometric baseline between the receiving telescopes on earth.

A. Atmospheric Refraction Models

For the model (11), the misassignment in the star position is a few mas for each kilometer of error in the scale height K . In the limit $K \rightarrow 0$, we recover the values for the flat earth of Eq. (1); the corresponding mathematical argumentation is given by (Stone 1996, (4)) and the limit $H^* \rightarrow 0$ in (Livengood et al. 1999, (1)). In practice, the scale height is coupled to the atmospheric gas density, and in a self-consistent model of a single average molecule species like Eq. (11), K is uniquely coupled to the atmospheric pressure at ground level (McCartney 1976).

In a variant of this problem, the scale heights of various gas components differ and their mixing ratios change. In this case, Eq. (11) would be upgraded to a sum over gas components with individual pairs of χ_0 and K —it is doubtful to scale the entire, single scale height with the ground humidity instead (Livengood et al. 1999). Consider for instance a fixed, “dry air” contribution to $\chi(r)$ with a constant scale height of 10 km at $\chi_0 = 4.0808 \cdot 10^{-4}$, superimposed by water vapor at $\chi_0 = 1.75 \cdot 10^{-6}$ that “freezes out” at scale heights of only a few kilometers: the pointing variations are $\approx 25 \mu\text{as}$ per km change in the water vapor scale height. Calibration of this water column could be achieved through monitoring spectral ranges of high atmospheric water absorption (Akeson et al. 2000; Meisner & Le Poole 2003).

The small difference in the refractive indexes at wavelengths of 2 and 2.4 μm , about $\Delta\chi_0 \approx 2.1 \cdot 10^{-7}$, displaces these two colored rays horizontally by about 0.80 mm if they hit the earth surface, calculated at apparent zenith angles of $z_0 \approx 30$ deg. If one looks at the starlight as an unvignetted plane wave, there is no such effect. Instead, there is a rainbow effect caused by this lensing of the earth atmosphere, which spreads the apparent positions of these two colors on the sky by 12.5 mas, which can be estimated through Eq. (1) as $\Delta R \approx \tan z_0 \Delta n$ using $\Delta n \approx \Delta\chi_0/2$ with Eq. (10). The calculation within the ray optics, however, can be used to consider the distortion/decorrelation induced by turbulence on length scales of these displacements (Colavita et al. 1987).

B. A Numerical Approach to the Refractivity Integrals

In the course of this investigation, the integrals (33) have been decomposed into refraction within the open interval $\rho \leq r < \rho + H$, plus one kink at $r = \rho + H$ where $\epsilon = n^2$ changes abruptly from 1 to $\epsilon_{r=\rho+H}$:

$$R_j = \frac{I^{2j+1}}{2} \int_1^{\epsilon_{r=\rho}} \frac{d\epsilon}{\epsilon(r^2\epsilon - I^2)^{j+1/2}} \quad (\text{B1})$$

$$= \frac{I^{2j+1}}{2} \int_{\epsilon_{r=\rho+H}}^{\epsilon_{r=\rho}} \frac{d\epsilon}{\epsilon(r^2\epsilon - I^2)^{j+1/2}} + I^{2j+1} \int_1^{n_{r=\rho+H}} \frac{dn}{n[(\rho+H)^2 n^2 - I^2]^{j+1/2}}. \quad (\text{B2})$$

The second term is Snell’s law in terms of the two angles of incidence, $\sin\psi_H \equiv I/(\rho+H)$ and $n_{r=\rho+H} \sin\psi_{H-} \equiv \sin\psi_H$ just above and below the atmosphere top boundary,

$$\int_1^{n_{r=\rho+H}} \frac{dn}{n\left(\frac{(\rho+H)^2 n^2}{I^2} - 1\right)^{j+1/2}} = \int_{\psi_{H-}}^{\psi_H} \tan^{2j} x \, dx = \begin{cases} \psi_H - \psi_{H-} & , j = 0 \\ \tan(\psi_H) - \psi_{H-} \dots & , j = 1 \\ \left[\frac{\tan^2(\psi_H)}{3} - 1\right] \tan(\psi_H) + \psi_{H-} \dots & , j = 2, \end{cases} \quad (\text{B3})$$

where the three dots mean the previous expression is to be subtracted with all ψ_H replaced by ψ_{H-} . The first term in Eq. (B2) is mapped onto the interval $0 \leq t \leq 1$ through the substitution

$$t = \gamma \frac{r - \rho}{r - \rho + H(1 - \gamma)}. \quad (\text{B4})$$

γ is chosen with the idea of important sampling such that $r_{1/2}$ —typically selected as 2 km—is mapped on $t = 1/2$. This yields $\gamma = (H - r_{1/2})/(H - 2r_{1/2})$ and leaves

$$\int_{\epsilon_{r=\rho+H}}^{\epsilon_{r=\rho}} \frac{d\epsilon}{\epsilon(r^2\epsilon - I^2)^{j+1/2}} = \gamma H(\gamma - 1) \int_1^0 \frac{\frac{d\epsilon}{dr} dt}{(t - \gamma)^2 \epsilon(r^2\epsilon - I^2)^{j+1/2}}. \quad (\text{B5})$$

This has been integrated with the trapezoidal rule, doubling the number N of equidistant sampling points after each step. As $\epsilon(r^2\epsilon - I^2)^{j+1/2}$ is a smooth function over the t -interval, the error in the trapezoidal rule is dominated by the variation in $(d\chi/dr)/(t - \gamma)^2$. For the exponential model (11) one can demonstrate that the sequence $V_N, V_{2N}, V_{4N}, \dots$, obtained by repeated division of the sampling step size by two, obeys $V_{4N} - V_{2N} \approx \frac{1}{2}(V_{2N} - V_N)$. The Richardson extrapolation induces the estimator $V \xrightarrow{N \rightarrow \infty} 2V_{2N} - V_N$, *not* the Simpson rule; monitoring the convergence of this estimator has been used to terminate the subdivision loop. A very similar analysis is applicable to the integrals v_i .

REFERENCES

- Abramowitz, M., & Stegun, I. A. (eds.) 1972, Handbook of Mathematical Functions (New York: Dover Publications), 9th ed.
- Akeson, R. L., Swain, M. R., & Colavita, M. M. 2000, in Interferometry in Optical Astronomy, edited by P. J. Lena, & A. Quirrenbach (Int. Soc. Optical Engineering), vol. 4006 of Proc. SPIE, 321
- Auer, L. H., & Standish, E. M. 2000, *Astron. J.*, 119, 2472
- Colavita, M. M., Shao, M., & Staelin, D. H. 1987, *Appl. Opt.*, 26, 4113
- Colavita, M. M., Swain, M. R., Akeson, R. L., Koresko, C. D., & Hill, R. J. 2004, *Publ. Astron. Soc. Pac.*, 116, 876
- Conan, R., Borgnino, J., Ziad, A., & Martin, F. 2000, *J. Opt. Soc. Am. A*, 17, 1807
- Filippenko, A. V. 1982, *Publ. Astron. Soc. Pac.*, 94, 715
- Green, R. M. 1985, *Spherical Astronomy* (Cambridge, London: Cambridge University Press)
- Gubler, J., & Tytler, D. 1998, *Publ. Astron. Soc. Pac.*, 110, 738
- Hui, L., & Seager, S. 2002, *Astrophys. J.*, 572, 540
- Karttunen, H., Kröger, P., Oja, H., Poutanen, M., & Donner, K. J. (eds.) 1987, *Fundamental Astronomy* (Berlin, Heidelberg: Springer)
- Langhans, R., Malyuto, V., & Potthoff, H. 2003, *Astron. Nachr.*, 324, 454
- Livengood, T. A., Fast, K. E., Kostiuik, T., Espenak, F., Buhl, D., Goldstein, J. J., Hewagama, T., & Ro, K. H. 1999, *Publ. Astron. Soc. Pac.*, 111, 512
- Mathar, R. J. 2004, *Appl. Opt.*, 43, 928
- McCartney, E. J. 1976, *Optics of the atmosphere: scattering by molecules and particles* (London, Sydney, Toronto: Wiley)
- Meisner, J. A., & Le Poole, R. S. 2003, in *Interferometry for Optical Astronomy II*, edited by W. A. Traub (Int. Soc. Optical Engineering), vol. 4838 of Proc. SPIE, 609
- Nener, B. D., Fowkes, N., & Borredon, L. 2003, *J. Opt. Soc. Am. A*, 20, 867
- Noerdlinger, P. D. 1999, *ISPRS J. Photogr. Rem. Sens.*, 54, 360
- Roe, H. G. 2002, *Publ. Astron. Soc. Pac.*, 114, 450
- Schonfelder, J. L. 1980, *Math. Comp.*, 34, 237
- Smart, W. M. (ed.) 1949, *Text-book on Spherical Astronomy* (Cambridge: Cambridge University Press)
- Stone, R. C. 1996, *Publ. Astron. Soc. Pac.*, 108, 1051
- Taff, L. G. (ed.) 1980, *Computational Spherical Astronomy* (New York, Rochester: Wiley)
- Tannous, C., & Nigrin, J. 2001, [arXiv:physics/0104004](https://arxiv.org/abs/physics/0104004)
- Thomas, M. E., & Joseph, R. I. 1995, *Johns Hopkins Apl. Technical Digest*, 17, 279